This is the accepted manuscript made available via CHORUS. The article has been published as:

# Electric field driven dynamic percolation in electronically phase separated (La_{0.4}Pr_{0.6})_{0.67}Ca_{0.33}MnO_{3} thin films

Hyoungjeen Jeen and Amlan Biswas

Phys. Rev. B **88**, 024415 — Published 16 July 2013

DOI: 10.1103/PhysRevB.88.024415

# Electric field driven dynamic percolation in electronically phase separated $(La_{0.4}Pr_{0.6})_{0.67}Ca_{0.33}MnO_3$ thin films

Hyoungjeen Jeen* and Amlan Biswas†

*Department of Physics, University of Florida, Gainesville, Florida 32611, USA*

## Abstract

Competing ferromagnetic metallic (FMM) and insulating phases in the manganite $(La_{1-y}Pr_y)_{1-x}Ca_xMnO_3$ leads to a phase separated state in which micrometer scale FMM regions behave in a fluid-like manner over a narrow temperature range. Here we show that an electric field can realign the fluid-like FMM phases embedded in an insulating matrix resulting in anisotropic in-plane resistance in microstructures of $(La_{0.4}Pr_{0.6})_{0.67}Ca_{0.33}MnO_3$ thin films. Time and voltage dependent resistance and magnetization measurements show that the dynamic percolation of the FMM regions leads to an insulator to metal transition due to electric field induced realignment of the FMM regions which is analogous to the dielectrophoresis of metallic particles suspended in fluid media. In-plane strain anisotropy plays an important role in determining the speed of dynamic percolation of the FMM regions by modifying the local electric fields in the phase separated state.

Magnetoelectric (ME) coupling in materials is a subject of interest both as a fundamental physics problem and for possible device applications [1, 2]. In materials with both magnetic and electric orders (multiferroics), ME coupling is defined as the effect of a magnetic/electric field on the electric polarization/magnetization and is usually small due to weak coupling between the mechanisms giving rise to magnetization and polarization [1]. In addition, the requirements for multiferroism in perovskite-type materials are often mutually exclusive [3]. An alternate route for controlling the magnetism with an electric field is offered in materials with centrosymmetric structures such as perovskite-type manganese oxides (manganites), where the ferromagnetic metallic phase is in competition with a non-ferromagnetic insulating phase close to a first order phase transition [4–6]. In the prototypical manganite $(La_{1-y}Pr_y)_{1-x}Ca_xMnO_3$, the competition among the ferromagnetic metallic (FMM), charge-ordered insulating (COI), paramagnetic insulating (PMI) phases leads to multiphase coexistence over a broad range of temperatures [4, 7] and makes it possible to tune their properties using external parameters such as magnetic field, electric field, and strain [8–11]. Electric field induced resistance changes are of particular interest and when resistance drops of several orders of magnitude were observed on the application of an electric field (colossal electroresistance or CER) in $(La_{1-y}Pr_y)_{1-x}Ca_xMnO_3$ [12–15], it was suggested that the effect was due to growth of the FMM regions which, if true, would be a unique form of ME coupling. However, magnetization measurements in the presence of an electric field ruled out such a scenario [13]. Monte Carlo simulations have shown that the observation of CER with no concomitant enhancement in magnetization could be due to electric field induced alignment of the FMM regions along the electric field direction [16]. If the model suggested by the simulations is correct then it could allow the manipulation of the shape (but not the volume) of the FMM regions using an electric field.

In this article we report an electric field driven insulator to metal transition due to the realignment of the FMM regions in phase separated $(La_{0.4}Pr_{0.6})_{0.67}Ca_{0.33}MnO_3$ thin films. Our observations suggest a mechanism similar to the dielectrophoresis (DEP) model of ref. [16]. We show that electric field induced dynamic percolation determines the anisotropic conductance in the thin film, and anisotropic strain (and the resultant magnetic anisotropy [17]) modifies the time scales of the electric field effect. Previous reports have claimed that strain driven anisotropic percolation is responsible for anisotropic resistivity in $La_{5/8-x}Pr_xCa_{3/8}MnO_3$ ($x = 0.3$) thin films [18]. However, these experiments were

carried out in magnetic fields of 6.5 tesla or higher and the electric field driven DEP-like behavior may have been suppressed. In addition, theoretical calculations have also shown that an electric field can lead to anisotropic resistivity and CER in the phase separated state of manganites [16, 19]. We observed the DEP-like behavior only in the fluid phase separated (FPS) region of the $(La_{0.4}Pr_{0.6})_{0.67}Ca_{0.33}MnO_3$ (LPCMO) phase diagram which corresponds to the same region of the phase diagram where strong electric field effects have been observed before [12, 13, 20]. On the other hand, in the glassy, static phase separated (SPS) region where the electric field effects are weak, DEP-like behavior is not observed. Our results show that the underlying mechanism of CER is the dynamic percolation of the FMM regions which are rearranged in a fluid-like manner in the manganite crystal lattice. In addition, our observations also introduce a new way to control the magnetism of centrosymmetric materials using an electric field.

20-nm-thick LPCMO thin films were grown on (110) $NdGaO_3$ (NGO) substrates using pulsed laser deposition as described in detail in ref. [17]. Fig. 1(a) shows an atomic force microscope (AFM) image of the film surface confirming the step flow growth mode with unit cell steps of $\sim$0.4 nm. The lattice mismatch strains at room temperature in the two in-plane directions are $\delta_{1\bar{1}0} = 0.49\%$ and $\delta_{001} = 0.26\%$ [17]. The epitaxial growth and composition of our thin films have been confirmed earlier using x-ray reflectivity, neutron reflectivity, and electron energy loss spectroscopy [11, 21]. We emphasize that these properties of the as-grown film minimize the possibility of extrinsic effects due to inhomogeneous strain and chemical inhomogeneities and we found that these qualities of our thin films are essential for the observation of anisotropic electric field effects. The $\rho$-$T$ for the as-grown thin film shows a sharp insulator-metal transition on cooling and a clear hysteresis between the cooling and warming cycles [17]. Magnetization measurements of a 30-nm-thick LPCMO thin film, grown under the same conditions, were performed using a Quantum Design 5 T Superconducting Quantum Interference Device (SQUID) magnetometer and show a clear strain induced magnetic anisotropy as shown in Fig. 1(b). The magnetization measurements also show that the in-plane magnetic anisotropy does not switch directions over the temperature range of this study, which is consistent with the fact that NGO does not show a structural transition in this temperature range [22] and that the average in-plane lattice contant of LPCMO is locked to the NGO substrate as the temperature is changed [18]. For the unpatterned thin films, the magnetic anisotropy does not lead to anisotropic resistivity [17].

It is possible that the absence of any resistivity anisotropy in the as-grown samples is due to the large sample size ($5 \times 5$ mm$^2$) compared to the micrometer scale phase separation in LPCMO [4, 7]. Monte Carlo simulations have indeed shown that multiphase coexistence leads to non-uniform electric fields which would prevent the detection of resistivity anisotropy in samples which are large compared to the scale of phase separation [16]. Hence, we reduced the sample size down to a $100 \times 250$ $\mu$m$^2$ cross structure as shown in Fig. 1(c). The structure was fabricated using a combination of photolithography and chemical etching [23]. Note that we carefully matched directions of the cross structure with the axes of magnetic anisotropy (as shown in Fig. 1(c)) to investigate possible contributions of this magnetic anisotropy. Phase separation on a scale as large as 10 $\mu$m has been observed in LPCMO thin films [7, 24]. However, for cross structures of smaller dimensions we were not able to reproducibly obtain insulator-metal transitions possibly due to presence of only the insulating phase in the small structure. Nevertheless, even for the $100 \times 250$ $\mu$m$^2$ structure, anisotropic transport was observed as shown in Fig. 1(d). The high resistance of the microstructure necessitated a two-probe, constant voltage resistance measurement as described in ref. [12]. The difference in the insulator-to-metal transition temperature while cooling ($T_{IM}$) along the two in-plane directions was about 1 K. Since the drop in resistance at $T_{IM}$ is about 5 orders of magnitude, if the resistance anisotropy is defined at $\frac{R_{hard}-R_{easy}}{R_{hard}} \times 100\%$, the maximum resistance anisotropy is $\sim 100\%$ (this definition of resistance anisotropy avoids values above 100%). An important feature of the resistance anisotropy is that it is observed only during the cooling cycle. It has been shown that the FPS state in which the FMM regions behave in a dynamic, fluid-like fashion, occurs only during the cooling cycle [7, 12]. Such dynamic behavior in the phase coexistence region has also been observed using magnetization, noise, and neutron diffraction measurements [25–27]. In the warming cycle, the phase boundaries are pinned and the FPS state is suppressed as has been directly shown using low temperature magnetic force microscopy [7]. Hence, we conclude that the fluidity of the FMM phase is necessary for the anisotropic resistance and the dynamic behavior of the FMM phase should reveal the true nature of the electric field effect.

To test the dynamic behavior of the resistance, we performed isothermal resistance measurements as a function of time ($R - t$). Fig. 1(e) shows the $R - t$ curves at 68.5 K for the two in-plane directions at a constant voltage of 30 V. The temperature of 68.5 K was chosen since it is slightly above $T_{IM}$ i.e. below the percolation threshold of the FMM phase

and to avoid resistance breakdown while ramping up the voltage to 30 V [7, 12, 28]. The anisotropic transport is revealed more clearly through this experiment since the breakdown time ($t_{BD}$), at which resistance suddenly drops due to the applied voltage, is an order of magnitude shorter along the $[1\bar{1}0]$ direction (magnetic easy axis) than that of the [001] direction (hard axis). The resistance drop at $t_{BD}$ is clearly irreversible and the sample needs to be heated to a temperature outside the hysteresis region in the $R(T)$ curve (about 130 K) to recover the high resistance values. The role of Joule heating needs to be ruled out in any electric field/current driven effect. The difference in $t_{BD}$ along the two different directions strongly suggests that Joule heating plays a negligible role in the $R-t$ measurements. We will present further evidence of the negligible role of heating effects later in this paper.

We also performed simultaneous magnetization vs. time ($M-t$) and $R-t$ measurements in a SQUID magnetometer to confirm that there is indeed no electric field induced increase in magnetization in the FPS state at $t_{BD}$. To obtain a measurable magnetization signal, we performed these experiments on an unpatterned 20-nm-thick film grown in identical conditions as the thin film for the cross structure. This film had a lower $T_{IM}$ of 60 K and the $M-t$ and $R-t$ measurements were taken at 68 K. We needed to measure the $R-t$ and $M-t$ data at a temperature 8 K higher than $T_{IM}$ because the scanning action of the SQUID resulted in small thermal fluctuations which combined with the 800 Oe field were enough to throw the sample into the metallic state for temperatures closer to $T_{IM}$. The sample was first cooled down in zero field from 150 K to 68 K. We then measured the $M-t$ in a field of 800 Oe applied along the easy axis. The 800 Oe field is well above the coercive field of about 300 Oe at 68 K and was applied to align the magnetic domains. The magnetization was measured using a single 4 cm scan of the SQUID magnetometer to minimize the effect of thermal fluctuations on the sample. Fig. 2 shows the $M-t$ data thus obtained after subtraction of the magnetization of the paramagnetic NGO substrate at 800 Oe. The sample was then heated back up to 150 K and zero field cooled to 68 K. A voltage of 30 V was then applied (distance between contacts was about 5 mm) along the magnetic hard axis and both $R-t$ and $M-t$ were measured in a field of 800 Oe. Fig. 2 shows that at $t = 232$ s there is a drop in resistance of about one order of magnitude due to the applied voltage but there is no significant change in the simultaneous magnetization measurement. In fact, the $M-t$ curves at 0 V and 30 V follow the same trend within the noise level of the measurement. These results are similar to the observations in ref. [13]. Since there is no observable increase in

the magnetization, we conclude that the electric field driven resistance drop is not due to an increase in the FMM volume fraction but due to the dynamic percolation of the FMM regions.

In Fig. 3, we show the voltage dependence of the dynamic percolation effect. Fig. 3(a) and 3(b) show the $R-T$ curves along the easy and hard axes, respectively at 5 V and 60 V. In both directions the $T_{IM}$ increases by about 2K for the higher applied voltage ($V_A$) and there was no significant change in $T_{MI}$ (metal-to-insulator transition temperature during warming) which is consistent with our hypothesis of that the dynamic percolation happens only in the FPS state. Fig. 3(c) and 3(d) show the dependence of the $R-t$ curves on $V_A$. In both directions $t_{BD}$ reduces with higher $V_A$ which is consistent with a dynamic percolation scenario [9, 13, 29]. This voltage dependent resistance breakdown is similar to the electric field driven dynamic percolation of conducting particles suspended in non-conducting polymers [30, 31]. Fig. 3(e) and 3(f) show the variation of $t_{BD}$ as a function of $V_A$ for the easy and hard axes, respectively. Along the easy axis, we also plotted the $t_{BD}$ vs. $V_A$ graph as a semi-log plot as shown in the inset of Fig. 3(e) and fitted it to a straight line. Such exponential behavior of $t_{BD}$ with $V_A$ has been observed during dielectrophoresis in systems with metallic particles suspended in a dielectric material [32]. The fitting function at 68.5 K is $t_{BD} = A\exp(-kV_A)$, where $A = 2221 \pm 1$ sec and $k = -0.098 \pm 0.002$ V$^{-1}$. Note that we observed similar behavior in different samples grown under same conditions. Due to the sharp resistance transition at $T_{IM}$, only a very narrow temperature range allowed us to obtain $t_{BD}$ vs. $V_A$ curves as shown in Fig. 3(e) and 3(f). The resistance breakdown was induced at a minimum voltage of 4 V in the time window of our measurement. However, along the hard axis, the time dependent responses are slower than along the easy axis for the same experimental conditions. The semilog plot in the inset of Fig. 3(f) shows that for the hard axis the $t_{BD}$ vs. $V_A$ curve deviates from an exponential behavior at lower $V_A$. The exponent ($k = -0.044 \pm 0.001$ V$^{-1}$) and prefactor ($A = 3459 \pm 1$ sec ) for the exponential fit confirm the slower kinetics along the hard axis. The drastic difference between the two directions suggests that forces in addition to the electrostatic force due to $E_A$ are responsible for the overall electric field effect. The existence of such additional forces is also suggested by the anomalous resistance upturn observed when $V_A$ was lower than 28 V (marked by the arrow in Fig. 3(d)).

To address the microscopic origin of the difference between the electric field effects along

the magnetic easy and hard axes and the observation of the resistance upturn within the context of existing theoretical models, we need to test the specific predictions of these models. The $R-t$ behavior described above can be explained if there is a collective rearrangement of the FMM phase in an electric field [9, 16, 29]. Such models explain the resistivity drop without a concomitant increase in magnetization (FMM volume fraction), as shown in Fig. 2 and also reported in ref. [13], by invoking an electric field induced anisotropic resistance due to preferential percolation along the electric field direction. To check for such anisotropic resistance, we performed simultaneous $R(t)$ measurements along the two in-plane directions of the cross microstructure. The measurement setup is schematically shown in the top inset of Fig. 4(a). A *dc* voltage ($V_{dc}$) was applied along one direction and the resultant current measured to obtain the resistance along that direction. The details of the measurement scheme is given in ref. [12]. The resistance in the orthogonal in-plane direction was measured by applying a small *ac* voltage ($V_{ac}$) of 1 $V_{rms}$ in that direction. An *ac* voltage was used to avoid picking up a *dc* voltage drop in the orthogonal direction due to the non-uniform electric field distribution in the phase separated state and to enable an accurate resistance measurement using a $V_{ac}$ low enough not to induce electric field effects. When we applied a high voltage ($V_{dc}$ = 30 V) along the *hard axis*, at $t$ = 1083 seconds there is a small and unexpected drop in resistance along the *easy axis* and a simultaneous resistance increase along the hard axis (Fig. 4(a)). This anomalous increase in resistance was also observed in Fig. 3(d) and is possibly related to a shape anisotropy of the nucleating FMM regions at the scale of the unit cell and the resultant non-uniformity of the electric fields [16]. We will discuss this matter further in the next paragraph. At $t$ = 1505 seconds, the expected drop in resistance of about two orders of magnitude is observed along the hard axis and there is a simultaneous rise in resistance along the easy axis (bottom inset of Fig. 4(a)). These data agree qualitatively with computational results which predict an increase of resistance along the direction perpendicular to the electric field due to realignment of the FMM phase along the electric field without an increase in the FMM phase volume. We also observed similar anisotropic resistance behavior when we applied the $V_{dc}$ along the easy axis, except that the initial anomalous resistance upturn feature was absent. Such anisotropic behavior again rules out any significant Joule heating effects.

The remaining question is the relation between the magnetic anisotropy and the anisotropic behavior of the observed dielectrophoresis. In ref. [18] it was suggested that the anisotropic

transport in a magnetic field was due to preferential seeding and growth along the magnetic easy axis. In contrast, low temperature conductive AFM (cAFM) experiments on our thin films have shown that the magnetic anisotropy does not play a role in the nucleation and growth of the FMM phase [33]. Since the cAFM measurements were performed in zero magnetic field, we conclude that for the zero magnetic field results presented here preferential nucleation and growth along the magnetic easy axis is not the reason for the observed anisotropic transport. In ref. [19] it was suggested that in the larger tensile strain direction, the Jahn-Teller (JT) interaction is weakened due to the Mn-O-Mn bond angle being closer to 180° whereas the double exchange (DE) interaction remains unaffected due to negligible bond length change. Such an anisotropic modification of the JT and DE interactions could lead to anisotropic FMM clusters at the scale of the unit cell with a slight elongation of the cluster in the direction of higher strain [19]. This slight shape anisotropy would lead to higher local electric fields along the higher strain (and in our case the magnetic easy axis) direction as shown schematically in Fig. 4(b) and 4(c). Hence, a cooperative effect could lead to a faster percolation along the higher strain direction. This cooperative effect would also explain the higher $T_{IM}$ along the easy axis and the initial anomalous resistance drop along the easy axis shown in Fig. 3(d) and Fig 4. Magnetic interactions between the nucleating FMM regions may also be expected to influence the anisotropic resistance. Experiments in magnetic fields and theoretical models which include magnetic interactions are needed to identify the possible role of such interactions in determining the resistance anisotropy.

In conclusion, we have observed electric field induced anisotropic transport in microstructures of LPCMO thin films. Time and voltage dependent resistance measurements show that the main driving force for the anisotropy is the collective rearrangement of the FMM phase under electric fields which realigns them along the electric field direction. Since these effects are observed only in the FPS state in which the FMM phase behaves in a fluid-like manner, our results on crystalline manganite films are analogous to dielectrophoresis of metallic particles suspended in fluid media [16, 34]. Anisotropic strain also plays an important role possibly due to the anisotropic shapes of the nucleating FMM regions at the scale of the unit cell which modifies the local electric field resulting in a cooperative effect and faster percolation along the high tensile strain direction. Since the FMM regions are metallic and magnetic, these electric fields effects can be used to generate magnetoelectric effects in such

centrosymmetric materials.

This work was supported by NSF DMR-0804452.

---

* Present address: Materials Science and Technology Division, Oak Ridge National Laboratory, Oak Ridge, Tennessee 37831, USA

† amlan@phys.ufl.edu

[1] S.-W. Cheong and M. Mostovoy, Nat. Mater. **6**, 13 (2007).

[2] M. Fiebig, J. Phys. D: Appl. Phys. **38**, R123 (2005).

[3] N. A. Hill, J. Phys. Chem. B **104**, 6694 (2000).

[4] M. Uehara, S. Mori, C. H. Chen, and S. W. Cheong, Nature **399**, 560 (1999).

[5] H. Kuwahara, Y. Tomioka, A. Asamitsu, Y. Moritomo, and Y. Tokura, Science **270**, 961 (1995).

[6] E. Dagotto, T. Hotta, and A. Moreo, Phys. Rep. **344**, 1 (2001).

[7] L. Zhang, C. Israel, A. Biswas, R. L. Greene, and A. de Lozanne, Science **298**, 805 (2002).

[8] S. Jin, T. H. Tiefel, M. McCormack, R. A. Fastnacht, R. Ramesh, and L. H. Chen, Science **264**, 413 (1994).

[9] A. Asamitsu, Y. Tomioka, H. Kuwahara, and Y. Tokura, Nature **388**, 50 (1997).

[10] K. H. Ahn, T. Lookman, and A. R. Bishop, Nature **428**, 401 (2004).

[11] S. Singh, M. R. Fitzsimmons, T. Lookman, H. Jeen, A. Biswas, M. A. Roldan, and M. Varela, Phys. Rev. B **85**, 214440 (2012).

[12] T. Dhakal, J. Tosado, and A. Biswas, Phys. Rev. B **75**, 092404 (2007).

[13] G. Garbarino, C. Acha, P. Levy, T. Y. Koo, and S.-W. Cheong, Phys. Rev. B **74**, 100401 (2006).

[14] N. K. Pandey, R. P. S. M. Lobo, and R. C. Budhani, Phys. Rev. B **67**, 054413 (2003).

[15] M. Tokunaga, Y. Tokunaga, and T. Tamegai, Phys. Rev. Lett. **93**, 037203 (2004).

[16] S. Dong, H. Zhu, and J.-M. Liu, Phys. Rev. B **76**, 132409 (2007).

[17] H. Jeen and A. Biswas, Phys. Rev. B **83**, 064408 (2011).

[18] T. Z. Ward, J. D. Budai, Z. Gai, J. Z. Tischler, L. Yin, and J. Shen, Nat. Phys. **5**, 885 (2009).

[19] S. Dong, S. Yunoki, X. Zhang, C. Şen, J.-M. Liu, and E. Dagotto, Phys. Rev. B **82**, 035118 (2010).

[20] J. Tosado, T. Dhakal, and A. Biswas, J. Phys.: Condens. Mat. **21**, 192203 (2009).

[21] S. Singh, M. R. Fitzsimmons, T. Lookman, J. D. Thompson, H. Jeen, A. Biswas, M. A. Roldan, and M. Varela, Phys. Rev. Lett. **108**, 077207 (2012).

[22] D. Savytskii, L. Vasylechko, A. Senyshyn, A. Matkovskii, C. Bahtz, M. L. Sanjuan, U. Bismayer, and M. Berkowski, Phys. Rev. B **68**, 024101 (2003).

[23] G. Singh-Bhalla, S. Selcuk, T. Dhakal, A. Biswas, and A. F. Hebard, Phys. Rev. Lett. **102**, 077205 (2009).

[24] M. H. Burkhardt, M. A. Hossain, S. Sarkar, Y.-D. Chuang, A. G. Cruz Gonzalez, A. Doran, A. Scholl, A. T. Young, N. Tahir, Y. J. Choi, S.-W. Cheong, H. A. Dürr, and J. Stöhr, Phys. Rev. Lett. **108**, 237202 (Jun 2012).

[25] L. Ghivelder and F. Parisi, Phys. Rev. B **71**, 184425 (2005).

[26] P. A. Sharma, S. B. Kim, T. Y. Koo, S. Guha, and S.-W. Cheong, Phys. Rev. B **71**, 224416 (2005).

[27] J. L. Garcia-Munoz, A. Collado, M. A. G. Aranda, and C. Ritter, Phys. Rev. B **84**, 024425 (2011).

[28] Y. Murakami, H. Kasai, J. J. Kim, S. Mamishin, D. Shindo, S. Mori, and A. Tonomura, Nat. Nanotechnol. **5**, 37 (2010).

[29] H. T. Yi, T. Choi, and S. W. Cheong, Appl. Phys. Lett. **95**, 063509 (2009).

[30] X. Tai, G. Wu, H. Yui, S. Asai, and M. Sumita, Appl. Phys. Lett. **83**, 3791 (2003).

[31] G. Wu, S. Asai, C. Zhang, T. Miura, and M. Sumita, J. Appl. Phys. **88**, 1480 (2000).

[32] Y. Yang, P. Gao, S. Gaba, T. Chang, X. Pan, and W. Lu, Nat. Commun. **3**, 732 (2012).

[33] S. Singh, M. R. Fitzsimmons, H. Jeen, A. Biswas, and M. E. Hawley, Appl. Phys. Lett. **101**, 022404 (2012).

[34] K. D. Hermanson, S. O. Lumsdon, J. P. Williams, E. W. Kaler, and O. D. Velev, Science **294**, 1082 (2001).

## FIGURE CAPTIONS

FIG. 1. (Color online) (a) A 1 × 1 $\mu m^2$ atomic force microscope image of a $(La_{0.4}Pr_{0.6})_{0.67}Ca_{0.33}MnO_3$ (LPCMO) thin film on an $NdGaO_3$ substrate. The vertical scale is 5 nm and the height of each step is about 0.4 nm. (b) Magnetization hysteresis loops along hard axis and easy axis at 50 K for a 30-nm-thick LPCMO thin film. (c) Optical microscope image showing the dimensions of the cross-shaped microstructure of an LPCMO thin film. The orientation of the substrate and the relative directions of the magnetic hard and easy axes are shown schematically above the image of the microstructure. (d) $R(T)$ curves of the LPCMO microstructure along the magnetic easy axis and hard axis. The arrows show the direction of temperature change.(e) Isothermal time dependent resistance curves along the magnetic easy axis and hard axis at 68.5 K.

FIG. 2. (Color online) $M(t)$ and $R(t)$ curves along the easy axis at 68 K in an 800 Oe field showing that the electric field induced drop in resistance has negligible effect on the magnetization.

FIG. 3. (Color online) $R(T)$ curves for two voltages along (a) easy axis and (b) hard axis. Voltage dependence of the $R(t)$ curves along (c) easy axis and (d) hard axis at 68.5 K. The arrow in (d) marks the anomalous increase in resistance along the hard axis. Breakdown time ($t_{BD}$) as a function of applied voltage ($V_A$) along (e) easy axis and (f) hard axis. Insets show semilog plots along (e) easy axis and (f) hard axis.

FIG. 4. (Color online) (a) Simultaneous $R(t)$ measurements at 68.5 K along the hard and easy axes. The arrow marks the initial anomalous resistance increase along the hard axis. The dashed box highlights the resistance increase along the easy axis simultaneously with the resistance drop along the hard axis, a magnified view of which is shown in the bottom inset. Top inset: Schematic diagram of the simultaneous transport measurement setup. $R_{s1}$ and $R_{s2}$ are standard resistors. Schematic diagrams showing the effect of the anisotropic shapes of the nucleating FMM phase on the local electric field when the external voltage is applied (b) along the magnetic easy axis and (c) along the hard axis.

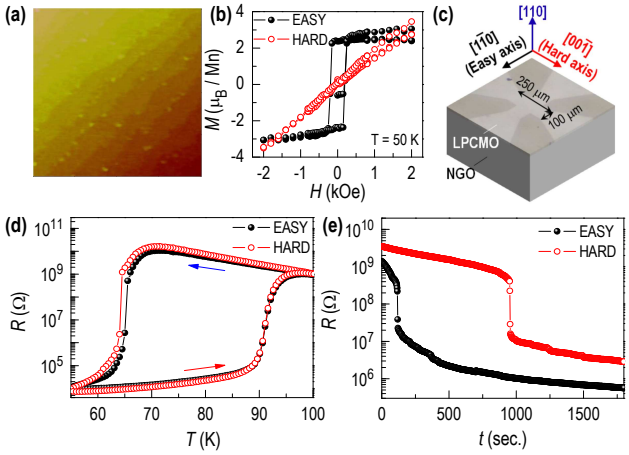
(a)
(b)
EASY
HARD
T = 50 K
M (μB / Mn)
H (kOe)
(c)
[110]
[1$\bar{1}$0]
(Easy axis)
[00$\bar{1}$]
(Hard axis)
250 μm
100 μm
LPCMO
NGO
(d)
EASY
HARD
R (Ω)
T (K)
(e)
EASY
HARD
R (Ω)
t (sec.)

FIG. 1.

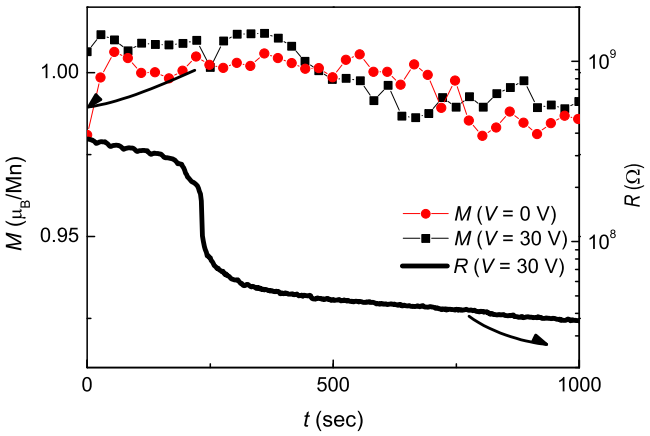


FIG. 2.

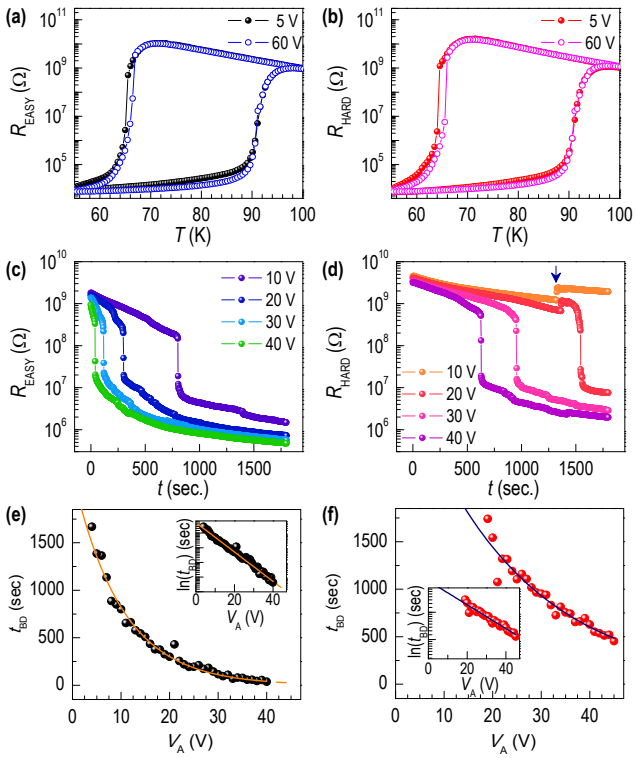


FIG. 3.

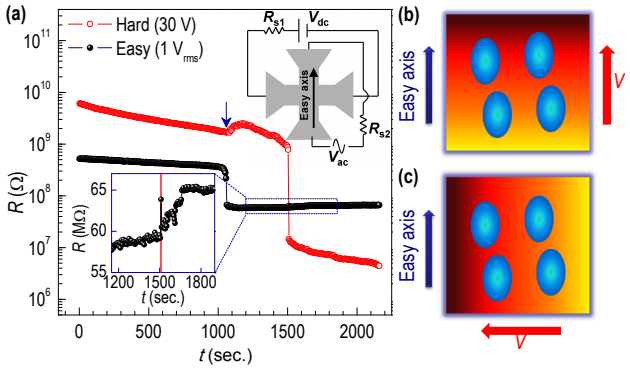
(a)
Hard (30 V)
Easy (1 V_rms)
R (Ω)
t (sec.)
R (MΩ)
t (sec.)
R_s1
V_dc
Easy axis
R_s2
V_ac
(b)
Easy axis
V
(c)
Easy axis
V

FIG. 4.